Journal of Pharmaceutical Analysis 12 (2022) 530–540

Contents lists available at ScienceDirect

Journal of Pharmaceutical Analysis

journal homepage: www.elsevier.com/locate/jpa

Review paper

Recent advances in ultrasound-controlled fluorescence technology for deep tissue optical imaging

Rui-Lin Liu [a, b, *], Ru-Qian Cai [a]

[a] School of Pharmacy, Xuzhou Medical University, Xuzhou, 221004, China
[b] Department of Pharmaceutical Analysis, School of Pharmacy, Xi'an Jiaotong University, Xi'an, 710061, China

ARTICLE INFO

Article history:
Received 7 May 2021
Received in revised form
13 September 2021
Accepted 9 October 2021
Available online 11 October 2021

Keywords:
Ultrasound-controlled fluorescence imaging
Temperature-sensitive NIR probes
High-resolution
Deep tissue
Molecular diagnosis

ABSTRACT

Fluorescence imaging is a noninvasive and dynamic real-time imaging technique; however, it exhibits poor spatial resolution in centimeter-deep tissues because biological tissues are highly scattering media for optical radiation. The recently developed ultrasound-controlled fluorescence (UCF) imaging is a novel imaging technique that can overcome this bottleneck. Previous studies suggest that the effective contrast agent and sensitive imaging system are the two pivotal factors for generating high-resolution UCF images ex vivo and/or in vivo. Here, this review highlights the recent advances (2015–2020) in the design and synthesis of contrast agents and the improvement of imaging systems to realize high-resolution UCF imaging of deep tissues. The imaging performances of various UCF systems, including the signal-to-noise ratio, imaging resolution, and imaging depth, are specifically discussed. In addition, the challenges and prospects are highlighted. With continuously increasing research interest in this field and emerging multidisciplinary applications, UCF imaging with higher spatial resolution and larger imaging depth may be developed shortly, which is expected to have a far-reaching impact on disease surveillance and/or therapy.

1. Introduction

Fluorescence imaging has gained significant attention as a noninvasive tool in basic studies and clinical applications [1]. It is a highly convenient and effective tool for real-time tracing of various fluorescence signals in biological applications because it can endow a high signal-to-noise ratio (SNR) and commendable spatial resolution during the imaging process [2]. In general, when light passes through biological tissue, the following light-tissue interactions can occur: photon reflection, photon scattering, photon absorption, and tissue autofluorescence (Fig. 1A). The main obstacles of fluorescence imaging include tissue autofluorescence, fluorescence quenching, photobleaching of the fluorescence photons, and poor tissue penetration [2]. Typically, fluorescence imaging is realized in the wavelength scopes from 400 nm to 700 nm (i.e., visible window) and from 700 nm to 1700 nm (i.e., near-infrared ray (NIR) window). However, NIR-fluorescence imaging offers more advantages, such as lower photon scattering and minimal autofluorescence interference [2]. More specifically, four biological windows are considered in the NIR region: NIR-I (700–900 nm), NIR-II (1000–1700 nm), NIR-III (1700–1870 nm), and NIR-IV (2100–2300 nm) windows. NIR fluorescence imaging with high resolution and satisfactory SNR exhibits immense potential in molecular detection and treatment applications [3].

In the past several decades, scientists have extensively explored fluorescence imaging in the NIR-I window from basic research to preclinical and clinical applications. Typically, the indocyanine green (ICG) and methylene blue as the US Food and Drug Administration (US FDA)-approved optical probes have been used for clinical applications. In recent years, fluorescence imaging in the NIR-II window has emerged as a new platform that provides higher SNR and deeper tissue penetration [2,4,5]. However, only a few fluorophores are available for NIR-II fluorescence imaging [6]. The existing NIR-II fluorophores have high hydrophobicity, poor photostability, and low quantum yield [2,6], which limit the development and practical applications of NIR-II imaging. Therefore, to boost the clinical translations of the NIR fluorescence imaging in deep tissue, especially to promote the investigations and applications of the US FDA-approved fluorophores, some novel NIR imaging techniques are urgently needed.

Peer review under responsibility of Xi'an Jiaotong University.
* Corresponding author. School of Pharmacy, Xuzhou Medical University, Xuzhou, 221004, China.
E-mail addresses: lrlxzmu@xzhmu.edu.cn, lrlxjtu1987@xjtu.edu.cn (R.-L. Liu).

https://doi.org/10.1016/j.jpha.2021.10.002

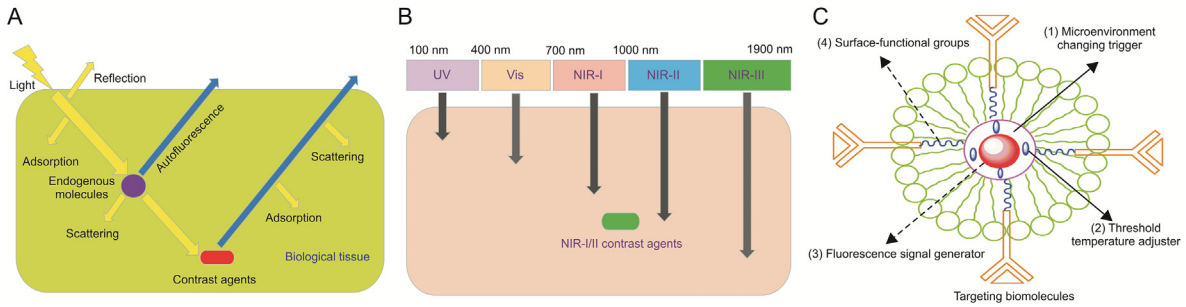

Fig. 1. (A) Schematic illustration of the interaction between light and tissue. (B) The schematic diagram of depth of penetration for the NIR-I/II light. (C) The UCF contrast agent's components. UCF: ultrasound-controlled fluorescence.

Compared with classical magnetic resonance imaging, computed tomography (CT), and positron emission tomography, NIR fluorescence imaging is a more effective, inexpensive, and ultrasensitive approach for real-time molecular imaging [6,7]. Presently, the poor resolution and insufficient penetration depth in deep tissues [1,6,8] are the primary factors that limit the universal clinical use of the NIR fluorescence technique. A particular issue is that the spatial resolution of the NIR fluorescence imaging sharply decreases with increasing tissue thickness [2]. In order to resolve this issue and obtain good spatial resolution for fluorescence imaging of deep tissues, several potential approaches were proposed. For instance, a combined broadband lock-in amplifier and fluorescent microbubbles has been used for detecting the signals of ultrasound-controlled fluorescence [9]. Luminescence imaging without an external excitation in a scattering medium [10] and the fluorescence imaging of temperature-responsive fluorescence probes [11] can all be adjusted by ultrasound. In addition, the ICG-loaded pluronic nanocapsules as both fluorescence intensity and lifetime probe were used for generating the ultrasound-controlled fluorescence images [12]. A combined light-pulse-delay and photon counting method can also be applied to obtain the ultrasound-controlled fluorescence images using a N-{2-[(7-*N*,*N*-dimethylaminosuflonyl)-2,1, 3-benzoxadiazol-4-yl] (methyl)amino} ethyl-*N*-methylacrylamide (DBD-AA) labeled poly *N*-isopropylacrylamide probe [13]. Meanwhile, scientists have explored the ultrasound-mediation of fluorescence imaging based on the bioluminescence and chemiluminescence mechanisms [14], and time-reversed ultrasonically encoded optical focusing that transmitting light into any defined location [15]. Nevertheless, the limited photons in the detected area restrict the acceptable sensitivity of NIR fluorescence imaging. The ultrasound-modulated tactics can realize good acoustic resolution in deep scattering media during the fluorescence imaging. However, manipulating the on/off signals of the NIR fluorescence imaging probe in living tissues via an ultrasonic modulator remains a significant challenge [16,17].

Ultrasound-controlled fluorescence (UCF) imaging can effectively address the issues mentioned above; thus, this technique has garnered considerable attention in recent years [16–21]. The unique UCF imaging probe with temperature-responsive property can be quickly unlocked via ultrasound-controlled approach only in the ultrasound confined space [17]. In addition, the UCF imaging system is different from the traditional fluorescence imaging system because the collected UCF signal is only derived from the signal changes of the UCF probe; in addition, the signal strength can be facilely adjusted by an ultrasonic modulator. Overall, the excellent UCF contrast agent and the sensitive UCF imaging system facilitate both ex vivo and/or in vivo high-resolution imaging [17]. Therefore, to develop a novel UCF probe and simultaneously build a sensitive UCF imaging system is a great challenge. To this end, some progress has been made, such as controlling the particle size, changing the components of UCF probes, and exploring new imaging modalities. However, no report has summarized the progress of this field in the past five years.

This review provides a detailed summary of the advances (2015–2020) in UCF imaging for deep tissue phantoms and in vivo imaging and offers a systematic approach that can be used to improve the UCF imaging system. Here, we briefly review the synthetic methods for UCF contrast agents and the emission characteristics, morphology, and surface characteristics of ICG-based UCF probes. The emerging applications of ICG-based UCF probes, including temperature-sensitive polymer nanoparticles (NPs) and thermosensitive liposomes, in the field of deep-tissue NIR fluorescence imaging, are also summarized. In addition, the advances of the UCF imaging system in the last five years are summarized. Finally, new opportunities and prospects for developing UCF imaging probes and UCF systems are discussed.

2. NIR-UCF imaging vs. traditional NIR imaging

Fluorescence imaging as a potential diagnostic tool displays good temporal-spatial resolution and high sensitivity; however, it faces the challenge of poor tissue penetration in the visible window (400–700 nm). In contrast, fluorescence imaging in the wavelength scope of 700–900 nm has some advantages, such as minimal tissue absorption, background fluorescence, and deeper tissue penetration [22]. Therefore, although NIR fluorescence imaging has received extensive attention as a noninvasive imaging technique in the past two decades, its practical applications are still restricted by limited tissue penetration and low spatial resolution [5]. The NIR-II fluorescence imaging has recently shown ameliorations in spatial resolution and imaging depth [23–28]. In particular, NIR-II fluorescent imaging can be used to probe centimeter-deep tissues and realize micrometer-scale resolution at depths of millimeters (Fig. 1B). However, all reported NIR-II fluorophores are slowly excreted and principally retained within the reticuloendothelial system, making clinical translation/application significantly difficult [23].

Compared with the traditional NIR fluorescence imaging, the UCF imaging technique has exhibited the significant potential to provide high-resolution fluorescence images for biomedical exploration. Specifically, the ultrasound-adjusted fluorescence strategy was first reported in 2006 [29]. Later, two independent research groups reported the utilization of the UCF imaging method in 2012 [11–13]. These groundbreaking developments facilitated an exciting future for high-resolution deep-tissue imaging based on fluorescence. In particular, Liu et al. [17] demonstrated that the poly (*N*-isopropylacrylamide) (PNIPAM)/β-cyclodextrin(β-CD)/ICG (PNIPAM/β-CD/ICG) nanogels as a potential UCF probe can be detected up to approximately 3.5 cm in the chicken breast tissue, which is better than the depths of previously reported NIR-I

[30–32] and NIR-II [1,24,33,34] contrast agents and close to the imaging depths of approximately 3.2 and 3.0 cm in pork tissue and slice pork ham using the NIR-I core/shell nanoparticles [35] and NIR chemiluminescence emitter [36], respectively. The earlier studies have also suggested that NIR-UCF imaging provides better SNR and spatial resolution as well as more comprehensive information (such as three-dimensional (3D) fluorescence images) on the deep tissues than conventional NIR-I technique, which can boost the synthesis of new NIR-UCF contrast agents within the NIR-I and NIR-II regions and further promote the biomedical applications of the NIR-UCF imaging.

3. Classification of NIR-UCF contrast agents

3.1. Composition and working mechanism of UCF contrast agents

A superior UCF contrast agent plays an important role in deep-tissue imaging with a high-resolution level. The UCF contrast agent generally contains four key components (Fig. 1C). 1) A trigger that changes the microenvironment of the UCF contrast agent. The temperature-sensitive polymer NPs or micelles such as PNIPAM or pluronic polymer have been used for achieving this goal because they exhibit excellent temperature-triggered phase transition [37,38]. 2) An adjuster that tunes the threshold temperature of the UCF contrast agent. The PNIPAM or pluronic polymer usually conjugates with a hydrophilic or hydrophobic compound to adjust the threshold temperature of the polymer. 3) A fluorescence emitter that generates the amplified fluorescence signal via increasing the temperature. A microenvironment-sensitive emitter, such as a polarity-sensitive fluorophore, is used for generating the “ON” fluorescence emission signal. 4) The surface-functional groups containing $-NH_2$, $-COOH$, and $-OH$ groups can interact with the targeting biomolecules [21], which facilitates the active targeting and aggregation efficiency of contrast agents to the lesion tissues.

The working mechanism of the UCF contrast agent involves the following steps. 1) The heat energy is first produced by high-intensity focused ultrasound (HIFU) technique; then, the confined temperature of the UCF probe is increased. 2) The internal microenvironment (i.e., hydrophilic characteristic) of the UCF probe is changed through the HIFU heating, which leads to a phase transition and weakening of polarity. Thus, the hydrophobic property of the UCF probe becomes stronger. 3) The quantum yield of the fluorophore increases with decreasing polarity, causing an enhancement in the absolute fluorescence intensity or fluorescence lifetime. That is, the emitted fluorescence from UCF probes is confined within the focused ultrasound region during UCF imaging. In contrast, weak or no fluorescence is produced when the UCF probes are located outside the focal volume. Therefore, the detected signal is observed as “ON” within the ultrasound confined volume because the background fluorescence in the “OFF” status is negligible without HIFU treatment. This also indicates that the spatial resolution of UCF imaging primarily relies on the size of confined thermal space. Besides, the outgoing fluorescence signal can be readily regulated by changing the ultrasound parameters and can only be generated from the confined UCF probes [39].

The in vivo NIR-UCF fluorescence imaging was first proved in a mouse model of breast tumor in 2019 [40]. In this groundbreaking work, the ICG-encapsulated PNIPAM (ICG-PNIPAM) NPs were used for in vivo high-resolution UCF imaging, which was conducted in mouse spleen via intravenous injections. It is important to explore stable and novel NIR-UCF imaging probes to further strengthen the development of in vivo UCF imaging. An NIR-UCF probe with multifunctional applications has the following properties: low toxicity, a reasonable on-to-off ratio of fluorescence intensity (I_{ON}/I_{OFF}), low critical solution temperature at around normal body temperature, narrow temperature transition bandwidth, high photo- and chemical-stability, and easy functionalization by targeted molecules or peptides for achieving specific targeting of lesion tissues. Until now, three types of NIR-UCF probes have been reported: temperature-sensitive polymer NPs [16], temperature-responsive micelles [17,21], and thermosensitive liposomes [39,41]. Only ICG-loaded thermosensitive liposome and ICG-encapsulated PNIPAM NPs have been triumphantly used for in vivo NIR-UCF imaging until now; other types of temperature-sensitive polymer NPs have not been reported yet. The temperature-responsive micelles including pluronic block copolymer such as pluronic F-98 and pluronic F-127 and linear PNIPAM polymer have been explored for utilization in UCF imaging. However, the existing pluronic nanoprobes are significantly difficult to realize in vivo UCF imaging because they are unstable in blood or tissue interstitial fluids [39]. The thermosensitive liposome is a potential UCF probe, which is generally fabricated by in situ hydration and self-assembly of lipids and NIR dyes [39]; in addition, its structure and size are tunable. Among these UCF contrast agents, the temperature-sensitive polymer NPs and thermosensitive liposomes have excellent biocompatibility. In addition, they are preferable in in vivo UCF imaging performance; hence, they exhibit a significant potential for future clinical translation. However, the active targeting effect of both contrast agents during ex vivo and/or in vivo UCF imaging has not been investigated yet. We focus on these two kinds of contrast agents (Table 1) in the following subsections.

3.2. Temperature-sensitive polymer nanoparticles

As a representative contrast agent, ICG-PNIPAM NPs (Table 1) have been used for NIR-UCF imaging [17]. The ICG-PNIPAM NPs with a spherical structure were initially prepared by free-radical polymerization in an aqueous medium where sodium dodecyl sulfate (SDS), ammonium persulfate (APS), and tetramethylethylenediamine (TMEDA) served as the surfactant, initiator, and accelerator, respectively [17,37]. ICG aqueous solution was premixed with the said polymer aqueous solution; ICG molecules with amphiphilic property were then encapsulated inside the SDS-based micelles. Finally, the ICG-PNIPAM NPs were obtained via a free-radical emulsion polymerization method under an inert atmosphere. In addition, the threshold temperature (either lower or higher) of the ICG-PNIPAM NPs could be tuned by conjugating with hydrophobic N-tert-butylacrylamide (TBAm) or hydrophilic acrylamide [37]. The storage time of ICG-PNIPAM NPs is below 30 days. In particular, the ICG dye can be easily oxidized by APS or TMEDA during the free-radical polymerization process. In order to overcome this limitation, the 4-4′-azobis (4-cyanopentanoic acid) (ACA) was used to replace APS and TMEDA as the initiator and catalyst, and synthesize the ICG-PNIPAM NPs [18]. The results indicated that the modified ICG-PNIPAM NPs had a good shelf life of 6 months. Meanwhile, considering the toxicity of the surfactant SDS, Yu et al. [18] also explored the pluronic F-127 or F-98 to replace SDS for fabricating the ICG-PNIPAM NPs. The toxicity of the ICG-PNIPAM NPs using pluronic F-127 or F-98 as a surfactant is still unclear.

In general, in vitro and in vivo tests are essential for evaluating the imaging performance of any contrast agent. For in vitro or ex vivo studies, Yu et al. [18] embedded a silicone tube (inner diameter = 0.76 mm) in a silicone phantom at a depth of ~5 mm to simulate a blood vessel. They inserted a small silicone tube (inner diameter = 0.31 mm) into a piece of porcine muscle tissue (thickness = 10 mm) to simulate a real tissue microenvironment. For both the above models, high quality ex vivo UCF images with good SNR were achieved by using ICG-PNIPAM NPs with ACA as the initiator. However, in vivo UCF imaging has not been realized using

Table 1
Overview of current NIR-UCF contrast agents.

Items	Used NIR dyes	Temperature tuner of the switchable threshold	The type of the temperature-sensitive polymer nanoparticles	The type of the thermo-responsive liposome	The type of the temperature-responsive micelles
Components	ADP-CA; ICG	TBAm; AAm; AH; AAc	ICG-PNIPAM	ICG-based DPPC	ICG/ADP-CA based pluronic F-98 and pluronic F-127
Targeting biomolecules	NR	NR	NR	NR	NR
Size	NR	NR	30–400 nm	Around 7.0 μm	NR
Long-term toxicity	Acceptable; safe	Deleteriousness	Unclear	Safety or hypotoxicity	Unclear

ADP-CA: aza-BODIPY; ICG: indocyanine green; AH: allylamine; AAc: acrylic acid; PNIPAM: poly(*N*-isopropylacrylamide); DPPC: 1,2-dipalmitoyl-*sn*-glycero-3-phosphocholine; NR: not reported.

the same probe. Later, Yao et al. [40] found that the ICG-PNIPAM NPs were moderately stable in the biological environment; they were mainly accumulated into the spleen of the mice. Meanwhile, the in vivo UCF imaging of mouse breast tumors and in vivo/ex vivo UCF imaging of the mouse spleen were successfully realized using ICG-PNIPAM NPs and frequency-domain (FD)-UCF system. The main disadvantages of this contrast agent are that the size is too large and the toxicity is unclear, and especially the targeted property is lacking.

For elucidating the above-mentioned results, the two-dimensional (2D) fluorescence planar image of the locally injected ICG-PNIPAM NPs in a mouse's breast tumor and the shell temperature of the mouse are shown in Figs. 2A and B [40]. Figs. 2C–F [40] show that the 2D-UCF images with an X–Y plane forming at different depths were also successfully obtained. In addition, the top, right, and front side views of the reconstructed three-dimensional (3D) CT image and 3D UCF image are shown in Figs. 2G–I and Figs. 2J–L [40], respectively. These results are consistent with the above inferences. An intravenous injection was used for verifying the in vivo UCF imaging using the same nanoprobe. The results showed that most of the ICG-PNIPAM NPs remained in the position of the mouse spleen; the peak of the fluorescence signal was reached at ~3–4 h after the intravenous injection of mixed contrast agents (Figs. 3A–C) [40]. Similarly, the 2D-UCF images (Ex/Em = 808/830 nm) of different depths at X–Y plane and the above-mentioned three views of the reconstructed 3D CT and 3D UCF images are shown in Figs. 3D–M [40]. The in vivo UCF imaging was also successfully realized in this work. Furthermore, it was indicated that the UCF contrast agents with a median hydrodynamic diameter (approximately 335 nm) were mainly distributed in the positions of the spleen and liver with the uptake of macrophages [42].

The in vivo UCF imaging has been successfully realized by using ICG-PNIPAM NPs. However, a key disadvantage of this probe is that its emission wavelength is lower than that of free ICG in water [17]. To improve the NIR emission property and increase the in vivo retention time of ICG-PNIPAM NPs, Liu et al. [17] fabricated a PNIPAM/β-CD/ICG nanogels. The size of the as-prepared aqueous nanogel with a globular-like shape was in the range of 40–200 nm, and the mean particle size was approximately 32.3 ± 0.7 nm (PDI = 0.307). The hydrodynamic size of the aqueous PNIPAM/β-CD/ICG nanogels (approximately 32 nm) was significantly decreased as compared to that of the reported ICG-PNIPAM NPs (approximately 335 nm) [40]. In particular, the locations of the strongest absorption peaks were similar for both aqueous PNIPAM/β-CD/ICG nanogels (approximately 770 nm) and ICG (approximately 785 nm) [17]. Similarly, the maximum emission peak of PNIPAM/β-CD/ICG nanogel (approximately 790 nm) was comparable to that of the ICG (approximately 810 nm) when they were excited at 680 nm, which is favorable for deep-tissue UCF imaging. They also obtained that the intensity of the absolute fluorescence was enhanced by augmenting the dosage of the β-CD/ICG complex. The aqueous PNIPAM/β-CD/ICG nanogel had a feasible switching feature. For example, the I_{ON}/I_{OFF} was nearly 4.4, and the phase-transition temperature was around 37.5 °C, which were crucial for acquiring high-quality UCF images. This synthetic strategy improved the stability of ICG via the host-guest interaction of β-CD and ICG molecules and promoted the switching efficiency and hemocompatibility of ICG-PNIPAM nanogels. However, we think that this synthesis strategy still has room for improvement via photopolymerization and in-situ in vivo biological orthogonal methods.

The PNIPAM/β-CD/ICG nanogels and the previous ICG-PNIPAM NPs were injected into 1.5 cm and 3.5 cm thick chicken breast tissues for inspecting the UCF imaging resolution. The results reveal that the SNRs of the UCF image for both the nanogels are better than that of the previously reported ICG-PNIPAM NPs. In particular, the NIR-UCF imaging depth of the PNIPAM/β-CD/ICG nanogels can be up to approximately 3.5 cm of the chicken breast tissue, which is better than the reported values for NIR-I [30–32] and NIR-II [1,4,33,34] contrast agents. In addition, it is comparable to the imaging depths of approximately 3.2 and 3.0 cm in pork tissue and slice pork ham using the NIR-I core/shell nanoparticles [35] and NIR chemiluminescence emitter [36], respectively. Although the in vitro experiments are a universal tool to explore the penetration depth, tests in animal models cannot be superseded.

The metabolism results reveal that the prepared PNIPAM/β-CD/ICG nanogels can rapidly accumulate inside the liver tissue. Moreover, they can be metabolized from the body through the synergistic route of the hepatic-renal scavenging. However, the in vivo NIR-UCF image in the location of the liver has not been obtained, and only the ex vivo NIR-UCF imaging has been realized. These results show that the physiologically stable nanogels can be retained in mouse livers, which opens the possibility of diagnosing liver-related diseases and exploring other biomedical applications in the future. The biodistribution data indicate that the PNIPAM/β-CD/ICG nanogels can efficaciously deposit the U87 tumor via the enhanced permeability and retention effect. Based on this phenomenon, the in vivo NIR-UCF imaging technique can provide much more 3D tumor information than the conventional 2D planar fluorescence imaging technique. In addition, the design and synthesis of the temperature-sensitive polymer NPs with active targeting property are still highly desired.

3.3. Thermosensitive liposomes

For in vivo UCF imaging, the thermosensitive liposome may be a more promising UCF probe carrier than the present temperature-responsive nanoparticles. First, the as-used NIPAM and 2,2-azobisisobutyronitrile during PNIPAM synthesis are toxic to living cells [43]. Second, the excitation and emission wavelengths of the aqueous β–CD/ICG-based nanogels (λ_{ex} = 770 nm, λ_{em} = 790 nm)

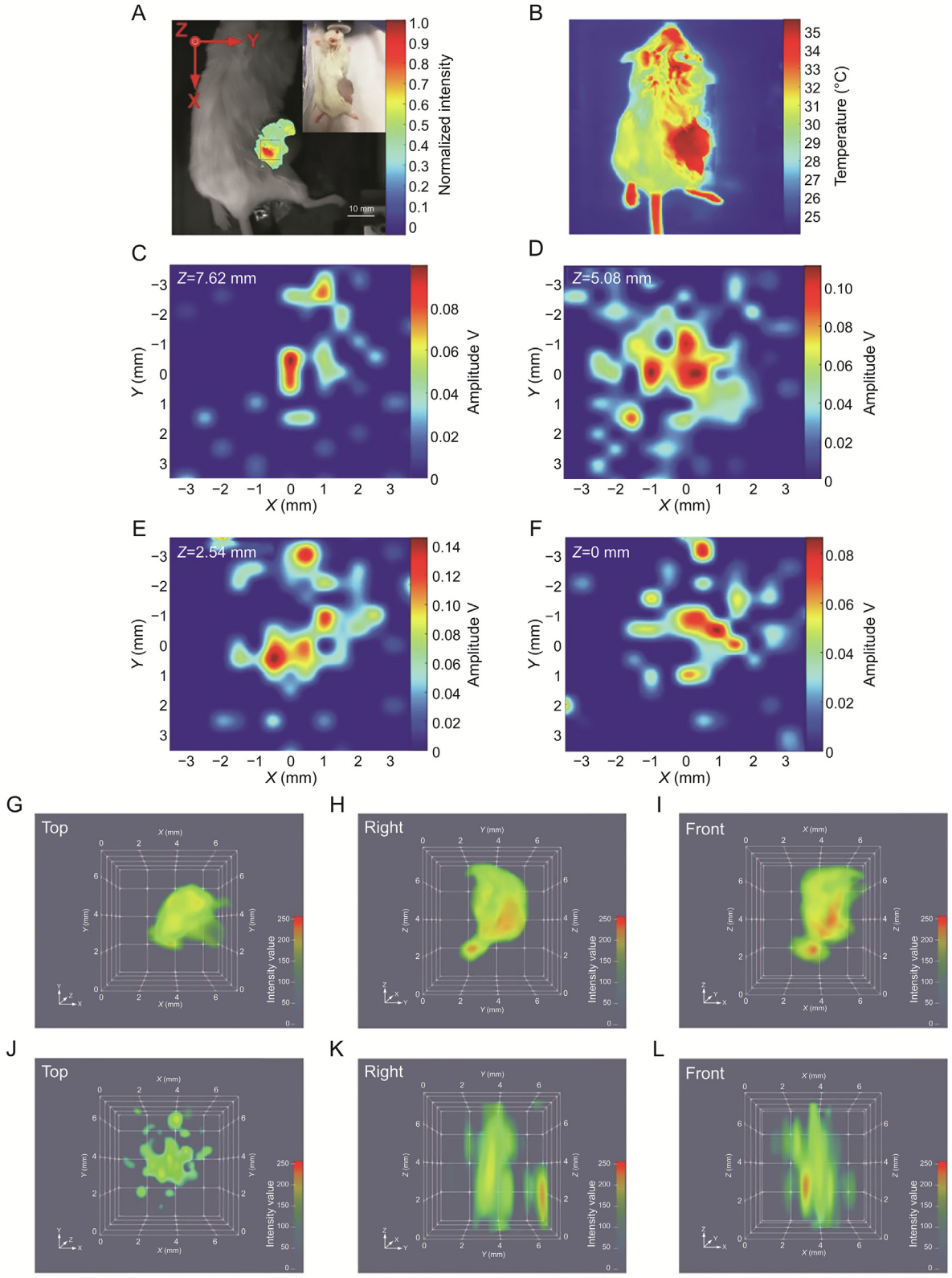

Fig. 2. (A) The fluorescence image of the mixed contrast agents via local injection in the tumor (Ex/Em = 808/830 nm). The top-right inset is the photograph of the mouse with a breast tumor. The red square is represented as UCF scan area. (B) A thermal imaging of the mouse. (C–F) 2D-UCF images of different depths at X–Y plane. (G–I) The top, right and front side views of the 3D CT image. (J–L) The top, right and front side views of the 3D UCF image. 2D: two-dimensional; 3D: three-dimensional. (Reprint with permission from Ref. [40].)

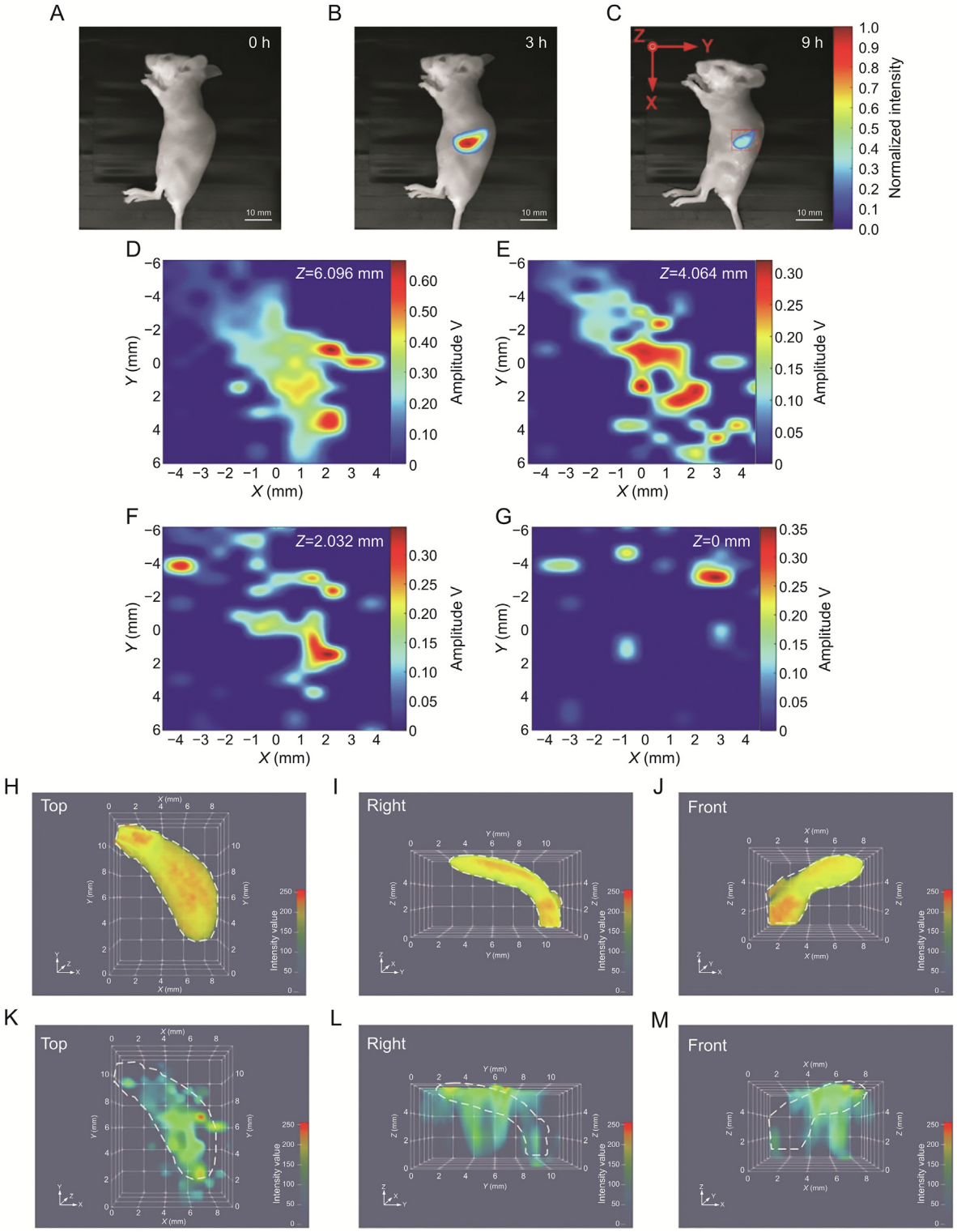

Fig. 3. (A–C) The 2D fluorescence images of the mouse at different times after intravenous injection of the mixed contrast agents. The red frame in (C) indicates the UCF scan area. (D–G) 2D-UCF images of the different depths at X–Y plane. (H–J) The top, right and front side views of the 3D CT image. (K–M) The top, right and front side views of the 3D UCF image. (Reprint with permission from Ref. [40].)

are still different from that of the aqueous ICG solution (λ_{ex} = 785 nm, λ_{em} = 810 nm) [17]. Finally, the current pluronic micelle-based probes are unstable in biological tissues; thus, it is significantly difficult to use them for in vivo UCF imaging [44].

Liposomes have a single or multiple phospholipid bilayer membranes outside the internal aqueous core [45]. They can be used to encapsulate hydrophilic drugs within the aqueous core, whereas lipophilic drugs can be incorporated into the membrane [46]. The size of the spherical vesicle is between micrometers and nanometers. In general, liposomes within the size range of 50–450 nm are employed in nanomedicine [47]. The size of the liposome is a key factor for clinical use. The relevant findings

indicate that the large-sized liposomes are quickly removed from the body [48].

In 2016, Zhang et al. [49] first reported that ultrasound can enhance the fluorescence signals of nanoscale excimer-emitting liposomes [49]. They used pyrene labeled on the fatty acid tail group or the head group of 1,2-dipalmitoyl-*sn*-glycero-3-phosphocholine (DPPC) phospholipids as the fluorochromes and unlabeled DPPC phospholipids as the carrier to prepare the liposomes via a freeze-thaw extrusion method. The results showed that the fluorescence emission intensity was increased when both the liposomes were exposed to ultrasound radiation. In 2017, Zhang et al. [41] developed a nanoscale ultrasound-switchable liposome fluorescent probe for NIR fluorescence imaging in optically turbid media based on the mechanism of the fluorescence resonance energy transfer (FRET) via ultrasound irradiation means. The results indicated that this method improved the image spatial resolution by 6.3 times as compared to that of the traditional fluorescence imaging. The FRET approach is independent of the variations in the local temperature, which is different from the previously reported UCF systems. In addition, the physiological stability and biodistribution of the dye-labeled liposomes and in vivo UCF imaging have not been explored yet.

In 2020, Liu and co-workers [39] used an ICG-liposome contrast agent for in vivo UCF imaging. Utilizing an evaporation-induced self-assembly method, they encapsulated an NIR ICG dye into the DPPC phospholipid membrane to fabricate the ICG-liposome. The as-prepared ICG-liposome (Table 1) with a size of around 7.0 μm had two LCSTs at 32 and 42 °C. To test the feasibility of the UCF imaging using the ICG-liposome probe, they embedded a silicon tube in a porcine muscle tissue as a tube model. The results validated the ability of the ICG-liposome in centimeter-deep tissue UCF imaging (1 and 1.5 cm). They also explored the UCF imaging in a tissue environment using ICG-liposome and commercial CT contrast agent and achieved good results in tissue and U87 tumor models. In addition, the in vivo tumor mouse model experiments indicate that the ICG-liposome can be effectively used for in vivo 3D UCF imaging inside a U87 tumor microenvironment. The biodistribution data show that the ICG-liposome is primarily accumulated at the lung, liver, and small intestines during the initial stage; then, it is transported to the liver and small intestines. The metabolic route reveals that most of the liposome-based probe is initially gathered in the liver, and then is tardily degraded and transported to the small intestines. The US FDA-approved DPPC and ICG were used in this work. Hence, the ICG-liposome is safe to use.

Although the ICG-liposome has been successfully used for ex vivo and in vivo NIR-UCF imaging, synthesis of the small-sized or nanoscale ICG-liposome with specific targeting functions still needs to be explored in the future. A smaller liposome with a larger surface area is significantly beneficial in bypassing biological barriers for blood vessel circulation [49]. In particular, the nanoscale ICG-liposome with active targeting characteristics for UCF imaging is highly desired in the future, which will significantly help in improving the sensitivity and temporal-spatial resolution of in vivo NIR-UCF imaging.

Overall, the success of in vivo UCF imaging primarily depends on the physiological stability of probes in biological tissues. In addition, the UCF probe with an excellent switchable property can ameliorate the SNR and reduce the required ultrasound power. Besides, an advanced and ultrasensitive UCF imaging system is also essential in generating high-quality UCF images. Such a UCF imaging system that can provide comprehensive 3D information is conducive to future biomedical research.

4. Advances in NIR-UCF imaging systems

In general, based on the variation in the fluorescence signal caused by ultrasound [21], the UCF imaging pattern is divided into two kinds: fluorescence intensity-based UCF imaging [37] and fluorescence lifetime-based UCF imaging (Fig. 4A) [13]. The existing studies show that high-resolution imaging of deep tissues can be achieved using both these imaging modalities. Herein, these imaging modalities are briefly reviewed.

4.1. Fluorescence intensity-based UCF imaging system

The working principle of the fluorescence intensity-based UCF imaging system is described as follows. First, the UCF contrast agents are injected into a silicone tubing within the biological tissue sample. An 808 nm semiconductor laser is used for continuously irradiating the superstratum of the tissue sample. The fluorescence signal of the NIR-UCF probes is generated under laser irradiation and passes through the biological tissue to the surface of the sample. Then, it is collected by a fiber bundle. The acquired fluorescence signal is transmitted through a specific filter and is further converted into the electrical signal via a photomultiplier tube (PMT); the electrical signal is displayed on an oscilloscope. The detected area of the sample is scanned by a focused ultrasound pulse in a point-by-point way. During the operation, the intensity and duration of the ultrasound pulse and the collection of fluorescence signals are manipulated by a pulse delay generator. The UCF images are finally reconstructed by the signals at each pixel. According to the above working mechanism, the resolution of UCF imaging is mainly influenced by the focal spot size of the focused ultrasound pulse. The imaging depth significantly depends on the switching multiple of the fluorescence signal and the SNR and sensitivity of the UCF imaging system.

The fluorescence intensity-based UCF imaging system was ameliorated by the same research group in 2016 [38]. Based on the previous UCF imaging system, they mainly implemented the following improvements (Fig. 4B) [38]. 1) The 808 nm semiconductor laser could be used to modulate the intensity of excitation light; the generated fluorescence signal was collected by using the phase-locked amplification technique. 2) The fluorescence signal was correlated with the frequency domain characteristics for differentiating the UCF signal. 3) The fluorescence intensity of the UCF probes could be enhanced more than 200 times by using focused ultrasound. The results indicated that a resolution of 900 μm was obtained in the 3.1 cm thick biological tissue phantoms.

Kandukuri et al. [50] reported a dual-modality imaging system containing UCF and B-mode ultrasound for acquiring the multicolor images and acoustic structure images of centimeter-deep tissue. A unique feature of this work is that they used two 90°-crossed focused ultrasound transducers with a superimposed focal region for realizing UCF imaging and ultrasound imaging on the X−Z plane. In the previous FD-UCF system, the emitted fluorescence photons of the UCF contrast agents are collected by a fiber bundle. Therefore, the collection of the emitted photon and the speeds of the scanning and imaging are inefficient. Because a raster scan is used in the FD-UCF systems, the tissue sample generally takes longer to cool before initiating data acquisition at the next scanning spot or location. A significant improvement in the UCF imaging system was validated by Yao et al. [20] in 2019. In this work, the optical detector of the UCF system was replaced by an electron-multiplying charge-coupled device (EMCCD) camera, and

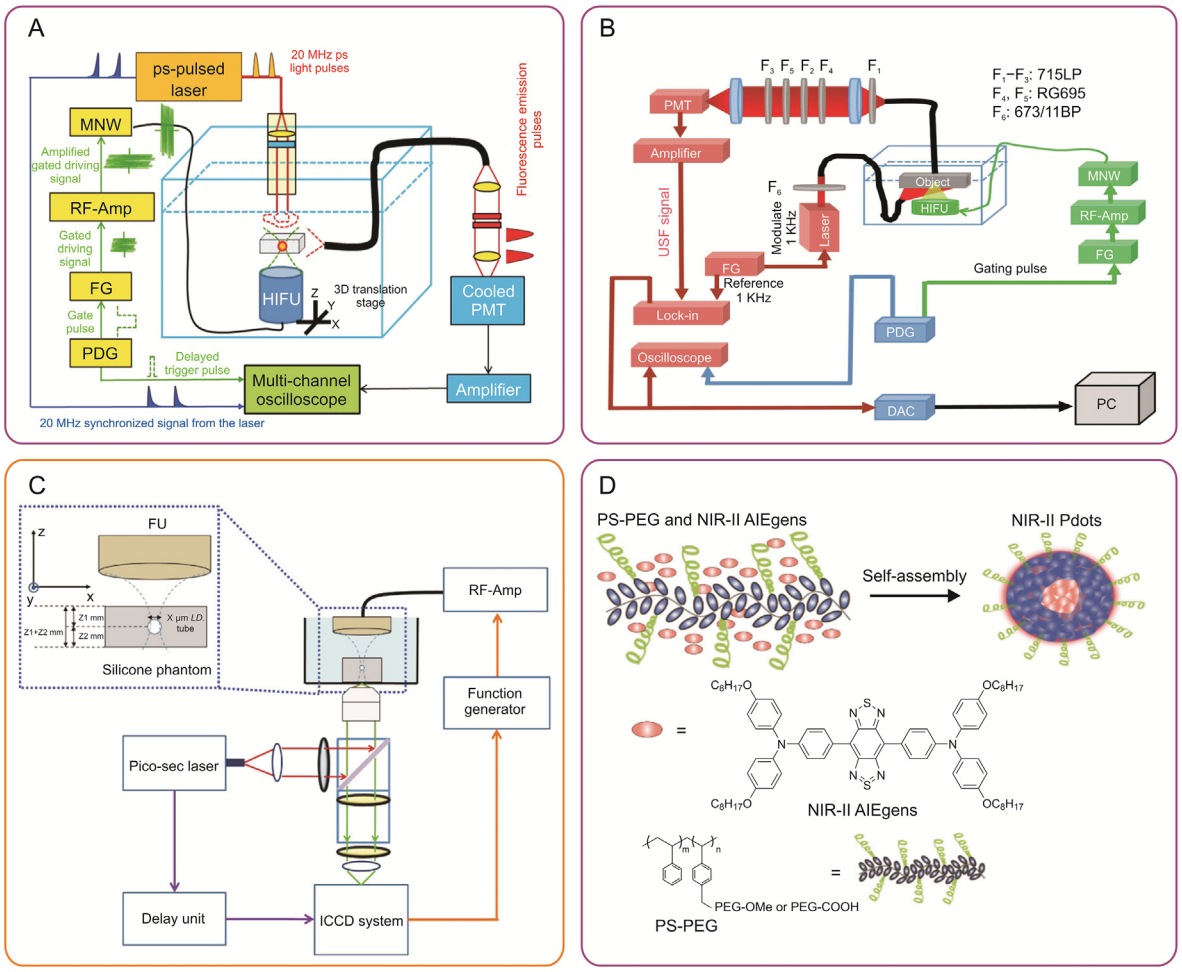

Fig. 4. (A) Illustration of the fluorescence lifetime-based UCF imaging system [13]. (B) Schematic diagram of the frequency-domain UCF imaging system with a fluorescence intensity readout [38]. (C) Illustration of ICCD camera-based time-domain UCF imaging system [51]. (D) Schematic of the preparation of NIR-II polymer dots [56]. EMCCD: electron multiplying charge coupled device; ICCD: intensified charge coupled device. (Reprint with permission from Refs. [13,38,51,56].)

the Z-scan method was adopted. Consequently, the imaging speed was promoted by four times over the previous raster scan, and the UCF imaging was further proved by using a micro-CT system. Subsequently, Yu et al. [51] developed an intensified charge-coupled device (ICCD) camera-based time-domain UCF imaging system for collecting high-quality UCF images (Fig. 4C). The laser device and ICCD camera were intelligently coupled into an inverted fluorescence microscope in this system. In 2020, Yu et al. [52] successfully obtained in vivo UCF images of the glioblastoma tumor by combining this ICCD camera-based imaging system and ICG-PNIPAM NPs with a particle size of approximately 330 nm. In particular, the 3D micro-mesoscopic information of lesion tissue was well presented.

Although several improved versions of the UCF imaging systems have been proposed, the emitted photons are usually collected by a single-fiber bundle and then transmitted to a PMT. Recently, Yao et al. [53] developed an EMCCD camera-based UCF imaging system. This system effectively surmounted the limitations of the previously reported UCF imaging systems. The differences between this new system and the previous UCF systems are as follows: 1) The exposure of the EMCCD camera was manipulated by a MATLAB software. 2) The photon collection efficiency and the imaging speed were enhanced by combining the EMCCD camera and Z-scan method. 3) The SNR and depth of NIR-UCF imaging were improved by employing the ICG-liposome and controlling the electron multiplying gain. In particular, the imaging depth could be up to 5 cm in chicken breast tissues. The findings on this newly designed EMCCD-UCF system indicated that the synthesized ICG-liposome (approximately 181 nm) had a better UCF imaging property than the previously reported PNIPAM/β-CD/ICG nanogels. In particular, the MATLAB trigger mode was more stable and intelligent than the hardware trigger mode for the electron multiplying gain. This work opens a new possibility for improving imaging speed and accurate imaging in tumor tissues. However, further research and validation for these challenging properties need to be explored in the future.

4.2. Fluorescence lifetime-based UCF imaging system

The enlargement of the fluorescence lifetime for the UCF probes under the HIFU radiation was initially reported by Yuan et al. [13] in 2012. As shown in Fig. 4A, a picosecond pulsed laser as the excitation light source was used to irradiate the sample in this imaging system. Typically, the temperature of the sample at the focus area of the acoustic field increased due to the ultrasonic radiation, leading to an increase in the fluorescence lifetime of the UCF probe. Thus, it was highly possible to identify the UCF signal by detecting the fluorescent photons after a specific delay time of the excitation light pulse. We note that the ability of this system to execute sub-millimeter-resolution deep-tissue imaging was proved in this

Table 2
Comparison of various UCF imaging performances during the period of 2012–2021.

System	SNR	Resolution	Imaging depth	Scan speed	Refs.
Fluorescence lifetime-based UCF system	ND	FWHM = 600 μm (depth-to-resolution is improved from 10 to 100)	20 mm optically turbid medium	Moderate	[13]
EMCCD-based UCF system	Resolution improved by 11 times	FWHM = 9.59 mm	Pig tongue tissue	Fast (4 times over the raster scan)	[20]
Fluorescence intensity-based UCF system	ND	FWEM = 0.68 mm in tube model	ND	Slow	[37]
Frequency-domain UCF system	17.6–242	900 μm	3.1 cm-thick biological tissue phantoms	Slow	[38]
Hybrid UCF and B-mode system	ND	FWHM = ~1.5 mm	14 mm-thick biological tissue phantoms	Moderate	[50]
ICCD-based time-domain UCF system	713	FWHM = 1.36 mm	Silicone phantoms	General	[51]
EMCCD-gain-controlled UCF system	(8.69–41.56) dB	FWHM = 1.65 mm	5.5 cm-thick chicken breast tissue	Faster	[53]
Ultrasound-pulse-guided digital phase conjugation	ND	Below 40 μm	2 mm-thick tissue phantoms	Moderate	[54]

SNR: signal-to-noise ratio; EMCCD: electron-multiplying charge-coupled device; FWHM: full width at half maximum; FWEM: full width at one eighth of the maximum; ICCD: intensified charge coupled device; ND: no data.

Table 3
Comparison of the ultrasound control conditions in various UCF systems during the period of 2012–2021.

System	Ultrasonic exposure time (ms)	Frequency of HIFU transducer (MHz)	Scanning mode	Scan area	HIFU driving voltage (mV)	Refs.
Fluorescence lifetime-based UCF system	100	2.5	X–Y plane	ND	ND	[13]
EMCCD-based UCF system	500	2.5	Z-scan	9.906 mm × 9.906 mm	60	[20]
Fluorescence intensity-based UCF system	300	2.5	X–Y plane	4.06 mm × 1.02 mm	ND	[37]
Frequency-domain UCF system	300	2.5	X–Y plane	ND	80 and 100	[38]
Hybrid UCF and B-mode system	ND	9	1-3D scanning	Overlapped focal region	ND	[50]
ICCD-based time-domain UCF system	400	2.5	X–Z plane	Scanning range of 3.96 mm, step size of 76.2 μm	70–160	[51]
EMCCD-gain-controlled UCF system	ND	2.5	Combined Z-scan and MATLAB trigger mode	8.128 mm × 4.064 mm	ND	[53]
Ultrasound-pulse-guided digital phase conjugation	ND	50	X–Y–Z plane	30 μm of step size	ND	[54]

HIFU: high-intensity focused ultrasound; EMCCD: electron-multiplying charge-coupled device; ICCD: intensified charge coupled device; ND: no data.

work. The SNR of the fluorescence lifetime-based UCF imaging is required to be higher than that of the fluorescence intensity-based UCF imaging [21], which is more attractive for high-quality UCF imaging. However, the relevant reports on this topic are rare. Therefore, novel NIR-UCF imaging techniques based on the fluorescence lifetime principle is still highly desirable for the monitoring and therapy of diseases.

Although various UCF imaging systems have been developed in the last few years, each imaging system has its advantages and disadvantages. A detailed comparison of the properties of various UCF imaging systems is shown in Tables 2 and 3 [13,20,37,38,50,51,53,54]. The newly developed EMCCD-gain-controlled UCF imaging system with high resolution, large scan speed, excellent SNR, and better imaging depth exhibits immense potential for in vivo UCF imaging and investigation on deep-tissue lesions. It will be useful for examining the vascular dynamics in animal models and understanding the cerebral diseases in deep tissues [55]. From the perspective of ultrasonic control conditions, the optimized parameters of the given HIFU conditions are also useful for improving the performance of the ex vivo or/and in vivo UCF imaging.

5. Conclusions and perspectives

Over the past few years, the UCF technique has been established as a novel tool to realize high-resolution fluorescence imaging in centimeter-deep tissues. One of its significant attributes is that it resolves poor spatial resolution in the deep tissues. Besides, a histological 3D image of the entire organ can be obtained by this imaging tool, which may provide useful insights into the tissue morphology, physiological processes, and the invasion and metastasis of tumors. Several ICG-based UCF probes have been excavated and used for ex vivo and/or in vivo NIR-UCF imaging. The thriving nanotechnology field can boost the design and synthesis of new UCF contrast agents. It has significant potential to exploit novel disease diagnostic methods in centimeter-deep tissues. In the present review, the recent advances (2015–2020) in the design and synthesis of the contrast agents and the improvements in the imaging systems for realizing high-resolution UCF imaging of deep tissues are summarized. In particular, recent progress in the evolution of the UCF probes, improvements in the UCF imaging systems, and in vivo UCF imaging are systematically explored.

Some key developments have occurred in this field. However, several challenges still limit the practical applications of in vivo UCF imaging technology: 1) limited polarity/temperature-sensitive NIR dyes and stable thermo-responsive polymer carriers, especially lack of the active targeting function; 2) poor stability and retention time of the UCF probes in vivo; 3) low on/off ratio of the UCF contrast agents; 4) potential toxicity of the developed UCF probes; 5) absence of highly sensitive and fast scanning UCF imaging systems; 6) optimization of such parameters, including the ultrasound control conditions and scanning model, might solve the current

problems. Therefore, further developments and in-depth investigations of the following are required to improve the diagnostic efficiency of in vivo UCF imaging technique and accelerate its clinical translation:

1) Exploring the feasibility of novel temperature-sensitive NIR dyes and thermo-responsive polymer carriers for the ex vivo and/or in vivo UCF imaging;
2) Integrating novel NIR dyes [56] into some intelligent temperature-sensitive carriers with negligible nanotoxicity and desired biocompatibility, and tailoring switchable properties;
3) Excavating the aggregation effect and biological mechanism of the UCF nanoparticles to target lesion tissues;
4) Evaluating the physiological stability and metabolism of the UCF probes;
5) Developing inexpensive and swift UCF imaging systems;
6) Incorporating acousto-optical tomography [57], NIR-II emissive polymer dots (Fig. 4D) [56] and aggregation-induced emission dyes [58] into UCF imaging technique may tackle some of the above-mentioned challenges;
7) From the clinical transformation point of view, the UCF technology still requires further development; the UCF imaging system with excellent and stable properties and NIR-UCF contrast agents with good biocompatibility are still being optimized and developed.

In our view, the current UCF imaging methods may more easily achieve clinical transformation in drug screening, liquid biopsy, and diagnosis and treatment of skin diseases. Moreover, the challenges can be addressed through multidisciplinary methods, including chemistry, biology, artificial intelligence, and material chemistry. These advances may provide valuable insights and ideas for designing new UCF probes and imaging systems and simultaneously facilitate their clinical applications in the targeted diagnosis of malignant tumors and detection of disease markers.

CRediT author statement

Rui-Lin Liu: Conceptualization, Writing - Original draft preparation, Reviewing and Editing, Funding acquisition; **Ru-Qian Cai**: Writing - Reviewing and Editing.

Declaration of competing interest

The authors declare that there are no conflicts of interest.

Acknowledgments

This review was supported by the National Natural Science Foundation of China (Grant No.: 81703466), the Outstanding Talents Research Start-up Fund of Xuzhou Medical University, China (Grant No.: RC20552107), and Xuzhou Science and Technology Bureau, China (Grant No.: KC21292).

References

[1] J. Qi, C. Sun, D. Li, et al., Aggregation-induced emission luminogen with near-infrared-II excitation and near infrared-I emission for ultra-deep intravital two-photon microscopy, ACS Nano 12 (2018) 7936–7945.
[2] S. He, J. Song, J. Qu, et al., Crucial breakthrough of second near-infrared biological window fluorophores: Design and synthesis toward multimodal imaging and theranostics, Chem. Soc. Rev. 47 (2018) 4258–4278.
[3] E. Hemmer, A. Benayas, F. Legare, et al., Exploiting the biological windows: Current perspectives on fluorescent bioprobes emitting above 1000 nm, Nanoscale Horiz 1 (2016) 168–184.
[4] S. Yu, D. Tu, W. Lian, et al., Lanthanide-doped near-infrared II luminescent nanoprobes for bioapplications, Sci. China Mater. 62 (2019) 1071–1086.
[5] D. Kim, N. Lee, Y. Park, et al., Recent Advances in inorganic nanoparticle-based NIR luminescence imaging: Semiconductor nanoparticles and lanthanide nanoparticles, Bioconjugate Chem. 28 (2017) 115–123.
[6] G. Hong, A.L. Antaris, H. Dai, Near-infrared fluorophores for biomedical imaging, Nat. Biomed. Eng. 1 (2017), 0010.
[7] J.A. Carr, D. Franke, J.R. Caram, et al., Shortwave infrared fluorescence imaging with the clinically approved near-infrared dye indocyanine green, Proc. Natl. Acad. Sci. U.S.A. 115 (2018) 4465–4470.
[8] J.V. Frangioni, *In vivo* near-infrared fluorescence imaging, Curr. Opin. Chem. Biol. 7 (2003) 626–634.
[9] B. Yuan, Y. Liu, P. Mehl, et al., Microbubble-enhanced ultrasound modulated fluorescence in a turbid medium, Appl. Phys. Lett. 95 (2009), 181113.
[10] N.T. Huynh, B.R. Hayes-Gill, F. Zhang, et al., Ultrasound modulated imaging of luminescence generated within a scattering medium, J. Biomed. Opt. 18 (2013), 20505.
[11] Y. Lin, L. Bolisay, M. Ghijsen, et al., Temperature modulated fluorescence tomography in a turbid media, Appl. Phys. Lett. 100 (2012) 73702–737024.
[12] Y. Lin, T.C. Kwong, L. Bolisay, et al., Temperature-modulated fluorescence tomography based on both concentration and lifetime contrast, J. Biomed. Opt. 17 (2012), 056007.
[13] B. Yuan, S. Uchiyama, Y. Liu, et al., High-resolution imaging in a deep turbid medium based on an ultrasound-switchable fluorescence technique, Appl. Phys. Lett. 101 (2012), 33703.
[14] J. Ahmad, B. Jayet, P.J. Hill, Ultrasound-mediation of self-illuminating reporters improves imaging resolution in optically scattering media, Biomed. Opt Express 9 (2018) 1664–1679.
[15] X. Xu, H.L. Liu, L.V. Wang, Time-reversed ultrasonically encoded optical focusing into scattering media, Nat. Photonics 5 (2011) 154–157.
[16] B. Cheng, V. Bandi, S. Yu, et al., The mechanisms and biomedical applications of an NIR BODIPY-based switchable fluorescent probe, Int. J. Mol. Sci. 18 (2017), 384.
[17] R. Liu, T. Yao, Y. Liu, et al., Temperature-sensitive polymeric nanogels encapsulating with β-cyclodextrin and ICG complex for high-resolution deep-tissue ultrasound-switchable fluorescence imaging, Nano Res 13 (2020) 1100–1110.
[18] S. Yu, B. Cheng, T. Yao, et al., New generation ICG-based contrast agents for ultrasound-switchable fluorescence imaging, Sci. Rep. 6 (2016), 35942.
[19] T.C. Kwong, A new modality for high resolution diffuse optical imaging: Temperature modulated fluorescence tomography [dissertation], Irvine: University of California, 2017.
[20] T. Yao, S. Yu, Y. Liu, et al., Ultrasound-switchable fluorescence imaging via an EMCCD camera and a Z-scan method, IEEE J. Sel. Top. Quant. Electron. 25 (2019), 7102108.
[21] Y. Pei, M.-Y. Wei, Newly-engineered materials for bio-Imaging technology: A focus on the hybrid system of ultrasound and fluorescence, Front. Bioeng. Biotech. 7 (2019), 88.
[22] Z. Ma, H. Wan, W. Wang, et al., A theranostic agent for cancer therapy and imaging in the second near infrared window, Nano Res 12 (2019) 273–279.
[23] A.L. Antaris, H. Chen, K. Cheng, et al., A small-molecule dye for NIR-II imaging, Nat. Mater. 15 (2016) 235–242.
[24] G. Hong, J.C. Lee, J.T. Robinson, et al., Multifunctional *in vivo* vascular imaging using near-infrared II fluorescence, Nat. Med. 18 (2012) 1841–1846.
[25] Y. Fan, F. Zhang, A new generation of NIR-II probes: Lanthanide-based nanocrystals for bioimaging and biosensing, Adv. Optical. Mater. 7 (2019), 1801417.
[26] Q. Zhang, H. Zhou, H. Chen, et al., Hierarchically nanostructured hybrid platform for tumor delineation and image-guided surgery via NIR-II fluorescence and PET bimodal imaging, Small 15 (2019), 1903382.
[27] H. Wan, H. Du, F. Wang, et al., Molecular imaging in the second near-infrared window, Adv. Funct. Mater. 29 (2019), 1900566.
[28] F. Ding, Y. Fan, Y. Sun, et al., Beyond 1000 nm emission wavelength: Recent advances in organic and inorganic emitters for deep-tissue molecular imaging, Adv. Healthc. Mater. 8 (2019), 1900260.
[29] M. Kobayashi, T. Mizumoto, Y. Shibuya, et al., Fluorescence tomography in turbid media based on acousto-optic modulation imaging, Appl. Phys. Lett. 89 (2006), 181102.
[30] J.Y. Zhao, D. Zhong, S.B. Zhou, NIR-I-to-NIR-II fluorescent nanomaterials for biomedical imaging and cancer therapy, J. Mater. Chem. B 6 (2018) 349–365.
[31] A. Yuan, J.H. Wu, X.L. Tang, et al., Application of near-infrared dyes for tumor imaging, photothermal, and photodynamic therapies, J. Pharmacol. Sci. 102 (2013) 6–28.
[32] U. Resch-Genger, M. Grabolle, S. Cavaliere-Jaricot, et al., Quantum dots versus organic dyes as fluorescent labels, Nat. Methods 5 (2008) 763–775.
[33] R. Bhavane, Z. Starosolski, I. Stupin, et al., NIR-II fluorescence imaging using indocyanine green nanoparticles, Sci. Rep. 8 (2018), 14455.
[34] Y.F. Wang, G.Y. Liu, L.D. Sun, et al., Nd^{3+}-sensitized upconversion nanophosphors: Efficient *in vivo* bioimaging probes with minimized heating effect, ACS Nano 7 (2013) 7200–7206.
[35] G.Y. Chen, J. Shen, T.Y. Ohulchanskyy, et al., (α-$NaYbF_4$:Tm^{3+})/CaF_2 core/shell nanoparticles with efficient nearinfrared to near-infrared upconversion for high-contrast deep tissue bioimaging, ACS Nano 6 (2012) 8280–8287.
[36] C. Liu, X. Wang, J. Liu, et al., Near-infrared AIE dots with chemiluminescence for deep-tissue imaging, Adv. Mater. 32 (2020), 2004685.
[37] Y. Pei, M.-Y. Wei, B. Cheng, et al., High resolution imaging beyond the acoustic diffraction limit in deep tissue via ultrasound-switchable NIR fluorescence, Sci. Rep. 4 (2014), 4690.

[38] B. Cheng, V. Bandi, M.Y. Wei, et al., High-resolution ultrasound-switchable fluorescence imaging in centimeter-deep tissue phantoms with high signal-to-noise ratio and high sensitivity via novel contrast agents, PLoS One 11 (2016), e0165963.
[39] Y. Liu, T. Yao, W. Cai, et al., A biocompatible and near-infrared liposome for *in vivo* ultrasound-switchable fluorescence imaging, Adv. Healthc. Mater. 9 (2020), 1901457.
[40] T. Yao, S. Yu, Y. Liu, et al., *In vivo* ultrasound-switchable fluorescence imaging, Sci. Rep. 9 (2019), 9855.
[41] Q. Zhang, S.P. Morgan, M.L. Mathe, et al., Nanoscale ultrasound-switchable FRET-based liposomes for near-infrared fluorescence imaging in optically turbid media, Small 13 (2017), 1602895.
[42] H. Boll, G. Figueiredo, T. Fiebig, et al., Comparison of fenestra LC, exitron nano 6000, and exitron nano 12000 for micro-CT imaging of liver and spleen in mice, Acad. Radiol. 20 (2013) 1137–1143.
[43] A.S. Wadajkar, B. Koppolu, M. Rahimi, et al., Cytotoxic evaluation of *N*-isopropylacrylamide monomers and temperature-sensitive poly(*N*-isopropylacrylamide) nanoparticles, J. Nanoparticle Res. 11 (2009) 1375–1382.
[44] H. Chen, S. Kim, W. He, et al., Fast release of lipophilic agents from circulating PEG-PDLLA micelles revealed by *in vivo* förster resonance energy transfer imaging, Langmuir 24 (2008) 5213–5217.
[45] M.A. Aghdam, R. Bagheri, J. Mosafer, et al., Recent advances on thermosensitive and pH-sensitive liposomes employed in controlled release, J. Contr. Release 315 (2019) 1–22.
[46] B. Kneidl, M. Peller, G. Winter, et al., Thermosensitive liposomal drug delivery systems: State of the art review, Int. J. Nanomed. 9 (2014) 4387–4398.
[47] M.L. Etheridge, S.A. Campbell, A.G. Erdman, et al., The big picture on nanomedicine: The state of investigational and approved nanomedicine products, Nanomedicine 9 (2013) 1–14.
[48] L. Sercombe, T. Veerati, F. Moheimani, et al., Advances and challenges of liposome assisted drug delivery, Front. Pharmacol. 6 (2015), 286.
[49] Q. Zhang, S.P. Morgan, P. O'Shea, et al., Ultrasound induced fluorescence of nanoscale liposome contrast agents, PLoS One 11 (2016), e0159742.
[50] J. Kandukuri, S. Yu, B. Cheng, et al., A dual-modality system for both multi-color ultrasound-switchable fluorescence and ultrasound imaging, Int. J. Mol. Sci. 18 (2017), 323.
[51] S. Yu, T. Yao, B. Yuan, An ICCD camera-based time-domain ultrasound-switchable fluorescence imaging system, Sci. Rep. 9 (2019), 10552.
[52] S. Yu, T. Yao, Y. Liu, et al., *In vivo* ultrasound-switchable fluorescence imaging using a camera-based system, Biomed. Opt Express 11 (2020) 1517–1538.
[53] T. Yao, Y. Liu, L. Ren, et al., Improving sensitivity and imaging depth of ultrasound-switchable fluorescence via an EMCCD-gain-controlled system and a liposome-based contrast agent, Quant. Imag. Med. Surg. 11 (2021) 957–968.
[54] K. Si, R. Fiolka, M. Cui, Fluorescence imaging beyond the ballistic regime by ultrasound-pulse-guided digital phase conjugation, Nat. Photonics 6 (2012) 657–661.
[55] M. Takezaki, R. Kawakami, S. Onishi, et al., Integrated fluorescent nanoprobe design for high-speed *in vivo* two-photon microscopic imaging of deep-brain vasculature in mice, Adv. Funct. Mater. 31 (2021), 2010698.
[56] X. Zhou, Q. Liu, W. Yuan, et al., Ultrabright NIR-II emissive polymer dots for metastatic ovarian cancer detection, Adv. Sci. 8 (2021), 2000441.
[57] J. Gunther, A. Walther, L. Rippe, et al., Deep tissue imaging with acousto-optical tomography and spectral hole burning with slow light effect: A theoretical study, J. Biomed. Opt. 23 (2018), 071209.
[58] J. Liu, F. Hu, M. Wu, et al., Bioorthogonal coordination polymer nanoparticles with aggregation-induced emission for deep tumor-penetrating radio-and radiodynamic therapy, Adv. Mater. 33 (2021), 2007888.